Preprints of the 21st IFAC World Congress (Virtual)
Berlin, Germany, July 12-17, 2020

Energy-Optimal Guidance of Hybrid Ultra-Long Endurance UAV

Vladimir N. Dobrokhodov, * **Claire Walton,** *
Isaac I. Kaminer, * **Kevin D. Jones** *

* *Naval Postgraduate School, Mechanical and Aerospace Engineering dept., Monterey, CA 93943 USA*
(e-mail:{ vndobrok, clwalton1, kaminer, jones}@nps.edu).

Abstract: The paper addresses the problem of calculating energy optimal trajectory for a novel class of hybrid UAV equipped with hydrogen fuel cell and solar photovoltaic energy production technologies. The objective of the design is to minimize the energy used for propulsion by optimally utilizing the finite energy stored in the onboard hydrogen fuel cell and routing the aircraft through the time-varying energy fields of solar irradiance and wind. The optimal guidance task is formulated as a two-point boundary value problem with an objective of finding the minimum energy route and the associated controls. The task is solved by applying Pontryagin minimum principle to the resulting 2D kinematics of a UAV along with its aerodynamics, energy management, and propulsion models. The paper derives the necessary conditions and synthesizes the optimal control laws of the bank angle and the airspeed which depend on the time and position derivatives of the wind, and the total angle of incidence toward the sun. The developed method is used to solve a task of path planning of a long endurance flight of a hybrid UAV over multiple 1000 nmi.

Keywords: Optimal guidance, Pontryagin minimum principle, solar and wind energy, hybrid vehicle.

1. INTRODUCTION

The paper addresses the problem of calculating energy optimal trajectory for an ultra-long endurance unmanned aircraft equipped with hydrogen fuel cell and solar photovoltaic technologies, see Fig. 1. The hybrid aircraft is currently in development at the US Naval Research Laboratory (NRL); it is designed to demonstrate long endurance (multiple days) and long range (more than 1000 nmi) in a small (7.3 m wingspan, 25 kg take-off weight) and mission-relevant vehicle, see Stroman et al. (2018). The project advances the aerial autonomy by integrating onboard a number of hardware and software solutions which enable the ultra-long endurance flight of a duration that cannot be achieved by each of the individual technologies. The anticipated range and endurance are achievable due to the tight integration of a unique hybrid power train that incorporates high specific energy (1200 Wh/kg) Proton-Exchange Membrane (PEM) fuel cell system, high efficiency (23%) solar arrays, and advanced power management, onboard trajectory planning and control algorithms.

Despite the long history of optimal control and specifically the optimal trajectory generation, the general class of tasks of finding the optimal trajectory for long-endurance flight is still an active area of research, see Ben-Asher (2010). The key reason for this ongoing development is twofold. First, the rapid evolution of aircraft design integrates new advances from various areas of aerospace engineering which have potential to extend the operational flight envelope. Achieving these potentials is solved by the optimal control methods that integrate all the advances along with the new flight critical dynamics and constraints. The second is the evolution of optimal control theory that provides new approaches, methods, and computational frameworks that facilitate the solution of the new or the previously intractable tasks. The use of optimal control methods for the aircraft trajectory generation has been comprehensively presented by the aerospace control literature, see Gardi et al. (2016); Ben-Asher (2010); Longuski et al. (2014). The complexity of the trajectory optimization task for the general class of aircraft, flight conditions, and the optimization cost has always challenged the formulation and the solution of the optimal control task. The first example of an optimal routing problem, also known as Zermelo's navigation problem, was proposed in 1931 by the German mathematician Ernst Zermelo, see Zermelo (1931). The problem is known in its aerospace version:

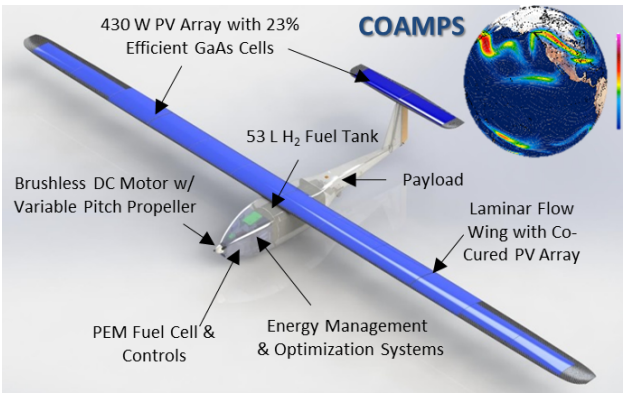

Fig. 1. A conceptual view of the long endurance energy harvesting system.

find a set of controls (heading and airspeed) under which the aircraft can optimally fly from one point to the other in minimum time in the presence of wind.

The optimal path planning for ultra long-endurance aircraft including the solar-powered and hybrid propulsion systems has been presented only by either qualitative discussions at the aircraft design stage, Burton and Hoburg (2017), or by the classical analysis that focused on steady-state flight performance characteristics, see Oettershagen et al. (2015, 2016). Nevertheless, high-fidelity models of a long endurance aircraft were built including the detailed representation of coupled aerodynamics and propulsion efficiency along with the solar and electric batteries models. By the time of this development, a sequence of works have addressed the solar energy impact on the trajectory shape. Seminal contributions to this problem have been made by Klesh and Kabamba (2007, 2009); Hosseini and Mesbahi (2016), which combine different flight modes of a solar-powered aircraft and enabled a solution of the trajectory optimization task, however without accounting for the wind transport energy.

A number of works attempted to combine the wind transport (primarily in 2D) and the solar energy of the aircraft but either for the individual narrow-sense costs (shortest time, distance traveled, fuel burned, weather as a hazard to the aircraft), see Rodionova et al. (2014), or their empirically weighted sum, Wirth et al. (2015). In all of these examples, the complexity of the task resulted in employing a direct formulation of the optimal control problem that relied on a form of computationally heavy nonlinear programming solvers. In most cases, the task was implemented in a general-purpose CPU by the Mathematica/MatLab programming languages that required 10-20 min of computational time with the power consumption starting at 60 W - prohibitive for microcontrollers.

However, the combined effect of the wind transportation energy and the solar irradiance has not been explicitly addressed. The key challenge is in the complexity of the optimization cost as well as the state and control constraints that together lead to the necessary conditions that rarely have analytical solutions. Direct and indirect methods are the key approaches capable of tackling this complexity without oversimplifying the problem. However, both approaches have one common problem of an initial guess; both frameworks require good initialization of the states and controls and in the indirect case also the associated costates, see a concise survey in Betts (1998). In essence, to solve the problem one needs to find an estimate of the "unspecified conditions at one end that produces a solution reasonably close to the specified conditions at the other end" Bryson and Ho (1975). A number of techniques, Watson (1990), have been developed to deal with this general sensitivity; among them are the scaling, continuation, and homotopy methods.

The present paper develops an integrated model of the aircraft kinematics along with the associated energy models that have the following original features. *First*, the energy collected and consumed is represented by coupled "bank angle & airspeed" nonlinear dynamics that account for all energy components including their efficiency as explicit functions of state during the flight. *Second*, the solar input is considered not only as a function of aircraft state and universal time, but also allows for the solar irradiance to be zero. Thus, the maneuvers in all light conditions are considered and day-night transitions are accounted for. Time-varying dynamics of wind, solar, and humidity (correlates to regional cloud cover) are given by COAMPS meteorological data model, see COAMPS (1997). *Next*, based on the integrated aircraft performance model, the problem of global path planning (GPP) of the solar-powered hybrid UAV is formulated as an optimal guidance problem, with the coupled bank angle and airspeed serving as the control inputs.

The paper studies this optimization problem and provides the following original contributions:

- the necessary conditions of optimality of the minimum energy are formulated;
- the optimal controls of the bank angle and the airspeed are synthesized analytically;
- the problem of initial guess is solved based on the continuation approach that scales the wind magnitude;
- an efficient algorithm is designed which is able to solve the GPP task onboard a miniature CPU consuming less than 5 W of energy within $10th$ of seconds;
- a practical task of an ultra long-endurance flight planning is solved for a prototype hybrid aircraft.

The paper is organized as follows. Chapter 2 formulates the mathematical models of the aircraft kinematics and the key energy components. Chapter 3 formulates the trajectory optimization task as the classical boundary value problem (BVP) and then synthesizes the optimal control laws of the bank angle and the airspeed. Chapter 4 presents the comparative analysis of the obtained energy optimal control laws and the classical Zermelo navigation task obtained with an exemplary wind profile. Finally, chapter 4 presents a solution that utilizes a realistic 4D weather forecast. Analysis of the result demonstrates the benefits of the energy optimal trajectory.

2. MATHEMATICAL MODELLING

Models of the aircraft and the environment. The aircraft control is based on the coordinated turn approach (bank to turn) for the aircraft flying at constant altitude within the planetary boundary layer (PBL). The difference in the horizontal turn kinematics with and without wind, see Beard and McLain (2012), is managed by an appropriately tuned autopilot that bounds the departure of the Euler yaw angle from the ground heading. Therefore, the airspeed V and the bank angle φ are considered as two controls.

Assumption A1: The aircraft is equipped with a stabilizing autopilot that makes the system in (1) a valid aircraft model.

Assumption A2: The long-endurance flight seeking for energy optimal strategy does not excessively use bank angle control, therefore it is also assumed that the bank angle is small and therefore $tan(\varphi) \approx sin(\varphi)$.

The aircraft model is:

$$\begin{aligned} \dot{x} &= V\cos\psi + W_x(x,y,t), \\ \dot{y} &= V\sin\psi + W_y(x,y,t), \\ \dot{\psi} &= g\tan\varphi/V_g, \\ V_g &= \sqrt{\dot{x}^2+\dot{y}^2}, \end{aligned} \tag{1}$$

where x and y are the Cartesian coordinates, ψ is the ground heading angle, φ is the bank angle, V is the airspeed, V_g is the ground speed, and g is the gravity. The W_x and W_y functions of position and time represent the mathematical model of the time-varying wind.

Power required for steady flight. Flight efficiency of the aircraft is based on the power required for steady-state flight at a constant altitude. On one hand, the constant altitude flight requires the weight of the aircraft to be compensated by the lift force: $L \cdot cos(\varphi) = m \cdot g$, where m is the mass and L is the total lift generated by the aircraft body. On the other hand, the total trust T of the propulsion system of a given efficiency η_p compensates for the drag force D acting on the aircraft at the given altitude h and airspeed V. Adopting the quadratic representation of the drag polar results in the following expression of the power required for steady flight:

$$\begin{aligned} &C_L = \frac{2mg}{\rho V^2 S \cdot \cos\varphi},\ C_D = C_{D_0} + K \cdot C_L^2, \\ &D = \frac{\rho V^2}{2} S C_D,\ T = D, \end{aligned} \tag{2}$$

where C_L, C_D, C_{D_0} are the aerodynamic coefficients of total lift, drag, and the drag at zero angle of attack respectively. K is the drag polar coefficient, and S is the reference area of the aircraft wing. Substituting these components into the propulsion power P_{prop} required for steady flight and accounting for the propulsion efficiency η_p results in the desired form of the energy loss model:

$$\begin{aligned} P_{prop} &= \frac{T \cdot V}{\eta_{prop}} = \rho V^3 S \cdot \frac{C_{D_0} + K \cdot C_L^2}{2\eta_{prop}}, \\ &= \frac{\rho \cdot S C_{D_0}}{2\eta_{prop}} \cdot V^3 + 2KS\frac{(mg/S)^2}{\rho \cdot \eta_{prop}} \cdot \frac{1}{V \cdot \cos^2\varphi}, \\ &= K_{p1} \cdot V^3 + K_{p2} \cdot \frac{1}{V \cdot \cos^2\varphi}, \\ K_{p1} &= \frac{\rho S C_{D_0}}{2\eta_{prop}},\ K_{p2} = \frac{2KS(mg/S)^2}{\rho\eta_{prop}}, \end{aligned} \tag{3}$$

where K_{p1} and K_{p2} are the propulsion system characteristic constants. As an example, the prototype aircraft features $K_{p1} \approx 0.05$ and $K_{p2} \approx 1000$.

Power gain due to solar. The solar power captured by the solar cells of known area A and efficiency η_{solar} is a function of the geographic location of aircraft (λ - latitude, ϕ - longitude, h - altitude), the orientation of the sun (a - azimuth and e - elevation), and the day of the year. The angle toward the sun is characterized by the incidence angle θ_i measured from the normal $\bar{n}_e$ to the solar cell, see Fig. 2. Thus, the solar power collected is

$$P_{solar} = \eta_{solar} P_{sd} A \cdot \cos\theta_i = K_s \cdot \cos\theta_i, \tag{4}$$

where $K_s = \eta_{solar} P_{sd} A$ and P_{sd} is the spectral density of the sun within the PBL altitude that is given by the solar flux layer of the COAMPS data; see COAMPS (1997) for more details on the quality and the content of the forecast. The $\cos\theta_i$ in (4) represents the magnitude of "solar power losses" due to the imperfect orientation of photovoltaic array toward the sun. As a reference, the prototype aircraft is characterized by $K_s \approx 400$.

The angle of incidence θ_i of the solar panel installed on an upper surface of the wing and oriented by the φ-roll, θ-pitch, and ψ-yaw angles of the aircraft body can be calculated by rotating the vector normal to the solar array to the Earth frame. The incidence θ_i is given by the vector dot product $\cos\theta_i = \bar{s}_e \cdot \bar{n}_e$ of the direction toward the sun ($\bar{s}_e$) and the normal to the solar array ($\bar{n}_e$), see Edwards et al. (2016); Klesh and Kabamba (2007).

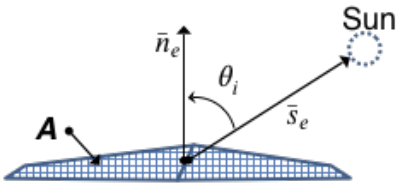

Fig. 2. The concept of solar incidence angle θ_i.

$$\cos\theta_i = \sin e \cos\varphi - \cos e \sin\varphi \sin(a - \psi). \tag{5}$$

The $\cos\theta_i$ of incidence angle modulates the solar power gained when the upper surface of the wing is illuminated by the sun. It can be observed that when the roll angle φ is small the value of $\cos\theta_i$ is primarily defined by the first term, therefore it can be approximated by $\cos\theta_i = \sin e \cdot \cos\varphi$. Moreover, when the sun is below the wing surface, $\cos\theta_i < 0$, the solar panels do not produce any power. The resulting function P_{solar} is written as:

$$P_{solar} = \begin{cases} K_s \cos\theta_i & ,\ if\ \cos\theta_i > 0 \\ 0 & ,\ if\ \cos\theta_i \le 0 \end{cases} \tag{6}$$

The orientation toward the sun is based on the traditional celestial mechanics equations, see Siegel and Moser (1995). The resulting azimuth and elevation angles (a, e) are the analytical functions of the sidereal rate of the Earth rotation ($\Omega = 15.041^o/hour$), solar time t_{sol}, and the latitude λ of the aircraft. The final form of these equations is adopted from Edwards et al. (2016) and presented here for completeness:

$$\begin{aligned} e &= \arcsin(\cos\lambda \cos\delta \cos\omega + \sin\lambda \sin\delta), \\ a &= sign(\omega) \cdot \arccos(\sin e \sin\lambda - \sin\delta)/(\cos e \cos\lambda), \end{aligned} \tag{7}$$

where $\omega = (t_{sol} - 12)\Omega$ is the hour angle corresponding to the solar time t_{sol}, and δ is the angular position of the sun at solar noon that is calculated empirically with respect to the day of the year, see Edwards et al. (2016).

Energy gain due to fuel cell. The power management concept of the hybrid aircraft does not focus on storing solar energy, rather it uses photovoltaic to offset the power production of the fuel cell to reduce the fuel consumption; P_{solar} never exceeds the P_{prop} of the prototype aircraft. Therefore, at any geographical location the power P_{net} required from the fuel cell for level flight is a function of the commanded airspeed V, bank angle φ of the solar wing, and the time of the day t:

$$\begin{aligned} P_{net}(V, \varphi, t) &= P_{prop} - P_{solar} \\ &= V^3 K_{p1} + K_{p2}/(V \cos^2\varphi) - K_s \cos\theta_i. \end{aligned} \tag{8}$$

The key objective function of the trajectory optimization task is the cumulative energy E_f spent during the flight:

$$E_f = \int_{t_0}^{t_f} (P_{prop} - P_{solar}) dt = \int_{t_0}^{t_f} P_{net} dt. \tag{9}$$

3. PROBLEM FORMULATION

The optimization task considers the constant altitude flight from an initial (x_0, y_0) position and time t_0 to the

final destination (x_f, y_f). The final time t_f is unknown and becomes a parameter of the BVP problem. The objective is to minimize the total energy expenditures in (9) by calculating the optimal commanded airspeed and bank angle. There are no tight constraints imposed on the control functions as the optimization of the flight performance naturally limits the control of the bank angle and the airspeed, see assumption A2. The formulation and solution of the optimal guidance is based on the Pontryagin minimum principle, see Pontryagin et al. (1962).

3.1 Minimum energy optimum control task.

minEng Problem: Find the optimal airspeed $V^\star$ and bank angle $\varphi^\star$ control functions that minimize

$$J^* = \int_{t_0}^{t_f} P_{net} dt \tag{10}$$

that is subject to the following state dynamics

$$\begin{aligned} \dot{x} &= V\cos\psi + W_x(x,y,t), \\ \dot{y} &= V\sin\psi + W_y(x,y,t), \\ \dot{\psi} &= g\tan\varphi/V_g,\ V_g = \sqrt{\dot{x}^2+\dot{y}^2}, \\ \dot{\tau} &= 1/t_f. \end{aligned} \tag{11}$$

The last "add-on"state in (11) introduces a "dimensionless time" τ that solves the ambiguity of unknown t_f and the normalized time becomes well-defined as $\tau \in [0,1]$.

3.2 Synthesis of the minimum energy optimal control laws.

Let the scalar Hamiltonian of the optimization task be:

$$\begin{aligned} H = {} & V^3 K_{p1} + K_{p2}/(V\cos^2\varphi) - K_s\cos\theta_i \\ & + \lambda_x\dot{x} + \lambda_y\dot{y} + \lambda_\psi\dot{\psi}, \end{aligned} \tag{12}$$

where the $\lambda_x, \lambda_y, \lambda_\psi$ are the costates associated with the dynamics of states in (11). The costates dynamics are now defined as:

$$\begin{aligned} \dot{\lambda}_x &= -\frac{\partial H}{\partial x} = -\lambda_x\frac{\partial W_x}{\partial x} - \lambda_y\frac{\partial W_y}{\partial x} - \lambda_\psi\frac{\partial\dot{\psi}}{\partial x}, \\ \dot{\lambda}_y &= -\frac{\partial H}{\partial y} = -\lambda_x\frac{\partial W_x}{\partial y} - \lambda_y\frac{\partial W_y}{\partial y} - \lambda_\psi\frac{\partial\dot{\psi}}{\partial y}, \\ \dot{\lambda}_\psi &= -\frac{\partial H}{\partial \psi} = \lambda_x V\sin\psi - \lambda_y V\cos\psi \\ & \quad + K_s\sin\varphi\cos e\cos(a-\psi) - \lambda_\psi\frac{\partial\dot{\psi}}{\partial\psi}, \end{aligned} \tag{13}$$

and the associated boundary conditions are:

$$\begin{aligned} x(t_0) &= x_0, \quad x(t_f) = x_f, \\ y(t_0) &= y_0, \quad y(t_f) = y_f, \\ \psi(t_0) &= \psi_0, \quad \psi(t_f) = \psi_f. \end{aligned} \tag{14}$$

Since the Hamiltonian in (12) is an explicit function of time, the resulting non-autonomous task has the following transversality condition at the right end

$$H_{t_f}(x, y, \psi, \tau\,\lambda_x, \lambda_y, \lambda_\psi) = 0. \tag{15}$$

The canonical Hamiltonian system is now built of (11,13) and the boundary conditions in (14,15).

Finally, all the partial derivatives of wind W_x, W_y , are available for calculation based on the COAMPS weather forecast, see COAMPS (1997); the derivatives of $\dot{\psi}$ with respect to (x, y, ψ, t), although bulky, are easy to implement as they are known functions of wind, V, and φ. Robustness of the optimal trajectory planner to the variation and uncertainty of weather forecast is achieved by the ability of the algorithm to quickly (1-2 min) recompute the optimal trajectory should the need arise.

With the states (x, y, ψ, t), control inputs (V, φ), and the Hamiltonian in (12), the first-order necessary conditions of optimality of the problem in (11-14) are:

$$\begin{aligned} \frac{\partial H}{\partial\varphi} = {} & \frac{2K_{p2}}{V}\cdot\tan\varphi(\tan^2\varphi+1) + \frac{\lambda_\psi}{V_g}\frac{g}{\cos^2\varphi} \\ & + K_s\sin\varphi(\sin e + \frac{\cos e\sin(a-\psi)}{\tan\varphi}) = 0, \end{aligned} \tag{16}$$

$$\begin{aligned} \frac{\partial H}{\partial V} = {} & 3V^2K_{p1} - \frac{K_{p2}}{V^2}(\tan^2\varphi+1) \\ & + \lambda_x\cos\psi + \lambda_y\sin\psi = 0. \end{aligned} \tag{17}$$

Utilizing the trigonometric identity $cos^{-2}(\varphi) = tan^2(\varphi)+1$ and the assumption A2 simplifies the (16):

$$\begin{aligned} \frac{\partial H}{\partial\varphi} = {} & \frac{2K_{p2}}{V}\cdot\tan\varphi(\tan^2\varphi+1) \\ & + K_s\tan\varphi(\sin e + \frac{\cos e\sin(a-\psi)}{\tan\varphi}) \\ & + \lambda_\psi\frac{g}{V_g}(\tan^2\varphi+1) = 0. \end{aligned} \tag{18}$$

Equation (18) can be considered as a polynomial of $\tan\varphi$ with the root closely approximated by (19) that represents the synthesized optimal control of the bank angle φ^*.

$$\tan\varphi^* = -\frac{V}{V_g}\frac{\lambda_\psi g + V_g\cdot K_s\cos e\sin(a-\psi)}{2K_{p2} + V\cdot K_s\sin e}. \tag{19}$$

The solution of the first-order necessary condition in (19) captures the key dynamics of the aircraft with respect to the wind energy and sun orientation (a, e) via the costate λ_ψ. Analysis of (19) shows that the ground speed of the aircraft should be non-zero at all times. This implies that the controls should always "cross-sail" the aircraft through the wind field and avoid direct headwind "collision". The remaining terms in (19) are treated as the aircraft state and performance characteristics.

Next, considering (17) and the assumptions A1-2 suggests that $tan^2(\varphi) \ll 1$. This simplifies (17):

$$\frac{\partial H}{\partial V} = 3V^4K_{p1} + V^2(\lambda_x\cos\psi + \lambda_y\sin\psi) - K_{p2} = 0. \tag{20}$$

On one hand, (20) suggests that within the scope of assumptions the airspeed (longitudinal channel) can be decoupled from the bank angle (lateral channel) control. On the other hand, the coupled time-varying energy contributions of solar and wind in (11-13) do not appear in the optimal airspeed control. Analysis of the costates dynamics in (12) shows that wind primarily contributes to the dynamics of λ_x, λ_y while the solar input affects λ_ψ. The scale of the resulting costates is defined by the relative magnitude of the wind transport energy and the solar irradiance. Finally, the expression of the optimal airspeed can be easily calculated by substituting the K_{p1}, K_{p2} terms from (3), thus leading to the following:

$$V^{*2} = \sqrt{\frac{4K}{3\rho^2C_{D_0}}(\frac{mg}{S})^2 + \frac{\eta_{prop}^2\Lambda^2}{9\rho^2S^2C_{D_0}^2}} - \frac{\eta_{prop}}{3\rho SC_{D_0}}\Lambda, \tag{21}$$

where $\Lambda = \lambda_x\cdot cos(\psi) + \lambda_y\cdot sin(\psi)$. It is worth noting that in the absence of solar and wind inputs the (21) reduces to the well-known expression of the optimal speed to fly for

the minimum required power V_{minP} in horizontal flight, see ch.5 in Anderson (1999).

$$V_{minP}^2 = \frac{2mg}{\rho S}\sqrt{\frac{K}{3C_{D_0}}} \tag{22}$$

How close the optimal control law of bank angle φ in (19) approximates the exact solution of $\frac{\partial H}{\partial \varphi} = 0$ for different combinations of the velocities and the orientation of the sun is illustrated in Fig. 3.

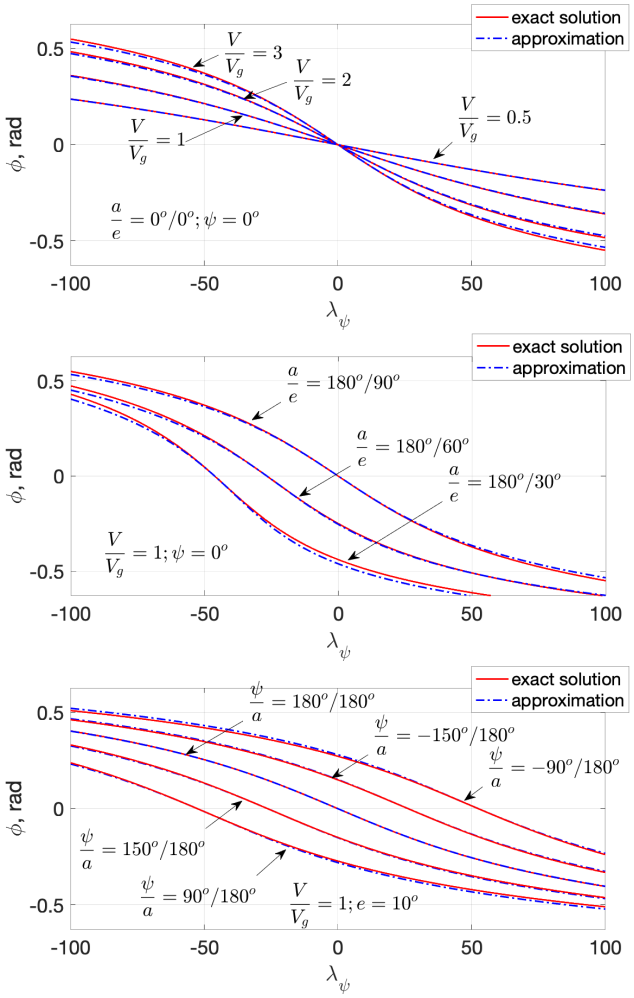

Fig. 3. The sensitivity of optimal bank control to the variation of velocities and the sun orientation.

It is clear that the optimal banking solution in (19) is both sensitive to the orientation of the sun and the ratio of the ground to airspeed, and represents very closely the exact solution; the latter one is obtained numerically via a computationally heavy numerical algorithm that would not be suitable for integration by the onboard BVP solver.

Equations (19,21) complete the formulation and synthesis of the *minEng* optimal control problem. The task of verifying the second order necessary conditions is addressed at the numerical implementation step, see details in Dobrokhodov et al. (2020). There, we develop a more intuitive means of analyzing the energy optimal solution by comparing it with the well-known minimum time (*minT*) and the shortest distance flights.

4. NUMERICAL SOLUTION OF THE GPP TASK

4.1 A. Challenges of numerical implementation.

One of the fundamental problems in solving the BVP task is to find the initial guess of the trajectory and the costates which is sufficiently close to the final solution. We solve this problem by designing a new continuation algorithm that is based on scaling the wind magnitude; this scale defines that physically meaningful parameter $W_{scale} \in [0, 1]$. The logic of the algorithm is illustrated in Fig. 4.

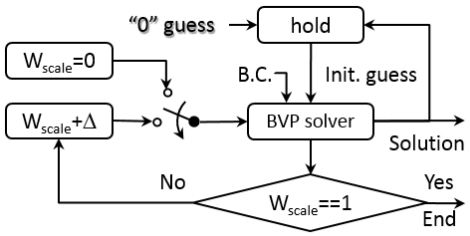

Fig. 4. The concept of continuation.

When $W_{scale} = 0$, meaning that there is no wind, the resulting trajectory is necessarily a straight line (an arc of a great circle) between the boundaries. The trivial initial guess of the adjoint variables ("0" guess) is a set of zeros. Then, a numerically stable forward integration of states and backward integration of costates solves the problem of initial guess of the very first trivial task. Thus, not only the states are defined, but also the costates of the BVP become available. As a result, continuously increasing W_{scale} from 0 to 1 and solving multiple BVP tasks shrinks the entire computational time to $10th$ of seconds vs multiple hours when using the full-scale wind as the initial step. The initial step of the BVP solver takes microseconds to compute on a single-board miniature ODROID-XU4 computer, see Hardkernel (2015). Over multiple iterations the CPU takes $10th$ of seconds depending on the variability of the wind that is being scaled up by the continuation procedure, while consuming merely 4.5 W that is $\approx$ 10 times less than Intel-i7, see Qureshi and Koubâa (2019).

The numerical solution relies on the $4th$ order collocation algorithm with the control of residuals, see Kierzenka and Shampine (2001), and is implemented by the MatLab, Mathworks (2019), and the SciPy software, see SciPy (2019). The onboard algorithm has been implemented by the authors in Python programming language to enable in-flight implementation of the GPP solver in Odroid CPU; MatLab core is not supported on ARM-based CPUs.

4.2 Comparative analysis of the minimum time and energy solutions with analytical wind representation.

The comparison was first performed for a wind profile defined analytically as it provides an easy assessment of the routes, controls, and the resulting energy metrics without any noise associated with real world weather data. An exemplary wind has been adopted from Bryson and Ho (1975); synthesized control of this task assumes constant wind. The wind is represented with one component being zero and the other being proportional to the lateral coordinate, thus switching its direction to the opposite when crossing the "zero line":

$$W_x(x, y, t) = -h_y \cdot y, \; W_y(x, y, t) = 0, \tag{23}$$

where h_y is a constant parameter representing the only non-zero partial derivative $\frac{\partial W_x}{\partial y} = -h_y$, see Fig. 5. This comparison is valid when performed with no sun contribution and the wind modeled as the time-invariant function.

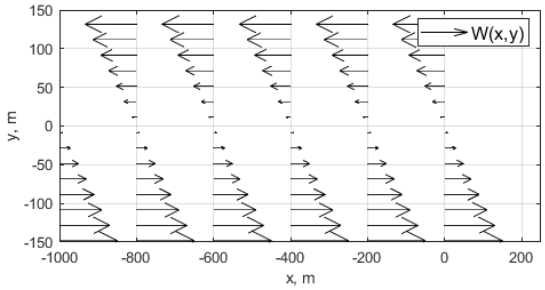

Fig. 5. Analytical wind, $h_y = 0.055s^{-1}$.

The focus of this comparison is to gain insight into the efficiency of harvesting the wind transport energy by both approaches. The plots in Fig. 6 compare the energy optimal solution ($minEng$) in (19,21) with the classical minimum time solution ($minT$) in terms of the trajectories, the bank angle, and the velocity controls in a simulated flight at night. The $minT$ task is solved with the airspeed of 11.85 m/s that matches the average speed of the $minEng$ solution. The scale of the trajectory plots in Fig. 6a is chosen to better demonstrate the negligible difference of both trajectories; the maximum difference is $\approx$ 50 m. The variation of optimal commanded airspeed in Fig. 6c due to the term Λ in (21) is minimal that is specific for the chosen wind model; the dynamic of Λ is driven by the costates λ_x, λ_y which depend on the partial derivatives of wind that in this example features only one nonzero component $\frac{\partial W_x}{\partial y}$. In general case, Λ is the term that blends the solar and the wind energies.

Analysis of Fig. 6 shows that the airspeed and the lateral controls are nearly identical for both solutions which are "flying" through the same wind at night. The bank angle dynamics are kept within 10^o limit. As expected, the resulting flight time (T_{minEng}/T_{minT} = 213/209 sec), the control efforts, and the energy expenditures (E_{minEng}/E_{minT} = 9.4/11.5 Wh) are nearly the same. The slight difference in the shape of trajectories and controls is primarily defined by the boundary conditions of the aircraft attitude; the $minEng$ case has ψ boundary at the ends while the $minT$ does not. Further analysis shows, that with the same wind conditions during the night flight, the $minEng$ trajectory asymptotically approaches the $minT$ solution that becomes especially pronounced with increasing distance between the boundary points. Therefore it is fair to generalize that at night time the $minEng$ solution closely approximates the $minT$ strategy.

To gain better insight into the combined contribution of wind and solar to the efficiency of flight, Fig. 7 illustrates the resulting solutions when the sun elevation angle varies between 0^o at night and 90^o at zenith. The cumulative variation of both controls results in less than 100 m difference in the trajectories for the two extremal cases of the sun elevation and is illustrated in Fig. 7a. The general trend is to increase the path length while also flying with higher airspeed that is afforded by the added

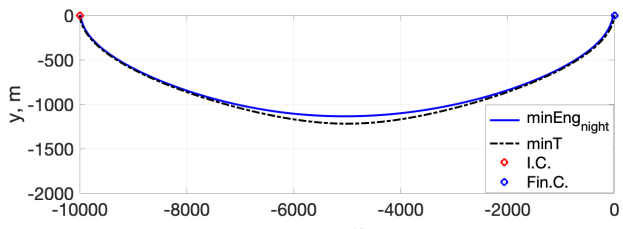

(a) trajectories

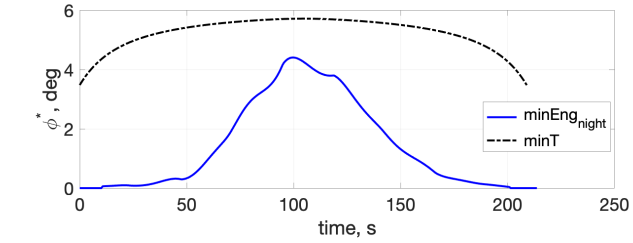

(b) bank control

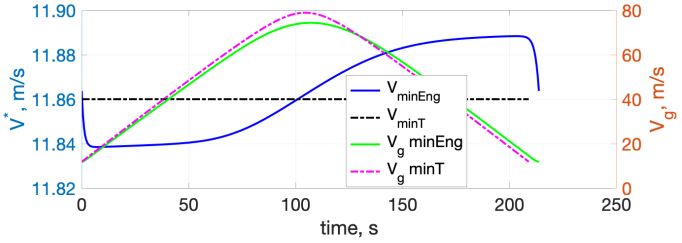

(c) the V and V_g velocities

Fig. 6. Comparison of $minEng$ and $minT$ optimal solutions at night flight.

contribution of solar, see Fig. 7b. The lateral control is trivial with the bank angle staying within 5^o in all cases, thus it is skipped here. The combined contribution of the wind and solar energies is illustrated by 10% increase of the ground speed, see Fig. 7c. Analysis of the paths and the velocities variation with the increased sun elevation (0^o-90^o) demonstrates decrease of the resulting flight time by 10%.

It is clear that the energy minimization strategy of the optimal control law relies on the maximum available solar energy, see Fig. 8. At night time it takes 9.4 Wh solely from the onboard fuel cell, while at 90^o elevation the onboard source utilization is reduced by 54%(4.3 Wh). Figure.8 also includes the total mass of fuel spent on the route that is computed by integrating the fuel consumption along the path. Analysis of this result in conjunction with the optimal flight speed in (22) explains the key performance gain of the energy optimal controls: additional solar energy allows for higher commanded airspeed that contributes to the higher ground speed and therefore the shorter flight time. The integral of the lower power consumption calculated over shorter flight time results in lower cumulative energy utilization.

4.3 Comparative analysis of the minimum time and energy solutions with wind represented by COAMPS model.

This section briefly presents a solution of a practical task of global path planning of a long endurance flight of the hybrid aircraft over more than 3000 nmi distance.

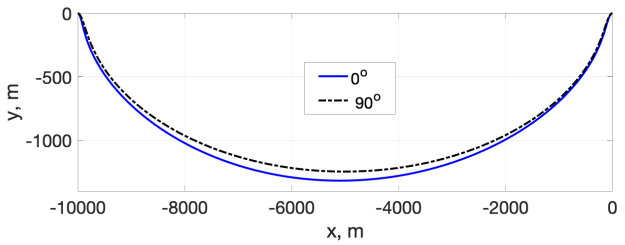

(a) trajectories

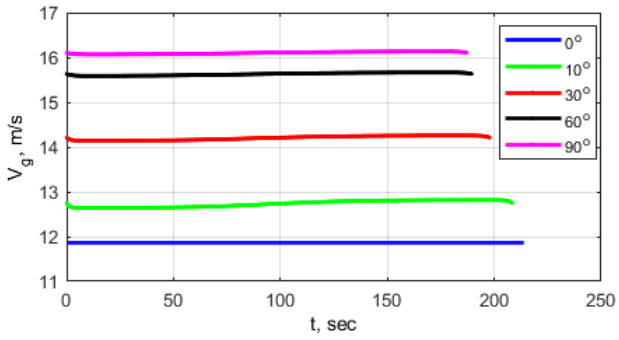

(b) commanded airspeed V

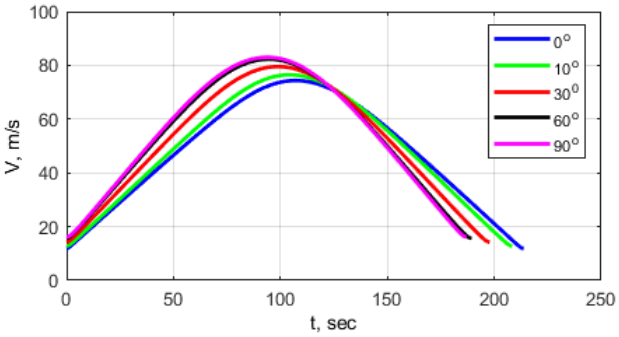

(c) resulting ground speed V_g

Fig. 7. Evolution of the trajectories and airspeed controls at various sun elevations

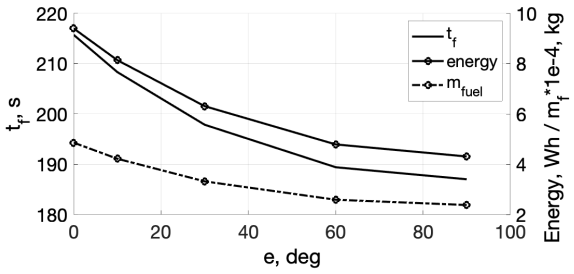

Fig. 8. Energy and flight time as functions of the sun elevation

It is expected that the flight time amounts to multiple days thus leading to the non-autonomous nature of the BVP task. Indeed, wind dynamics cannot be assumed to be independent on time. As a result, the classical Zermelo solution, which is autonomous, cannot be used in the comparative analysis. To facilitate fair analysis, the discussion uses the trajectory along the shortest path that is the arc of a great circle passing through the boundary points; it is conveniently calculated by the very first step of the continuation algorithm. The commanded airspeed along the arc will be fixed at the best speed to fly for minimum power, see (22). This great arc trajectory is a convenient reference for comparison. More details on the experiment and the developed interpretation of the results can be seen in Dobrokhodov et al. (2020).

Accounting for the time-varying nature of wind and solar energy fields along the route we introduce a special color-coding technique that helps with the intuitive representation of both energy sources (wind and solar). In the wind energy case, the algorithm calculates a projection of wind vector with respect to the direction of flight, see Fig. 9. The objective is to illustrate the strength of the wind magnitude and direction with respect to the commanded airspeed and the direction of flight, in other words - the quality of wind as the headwind or the tailwind.

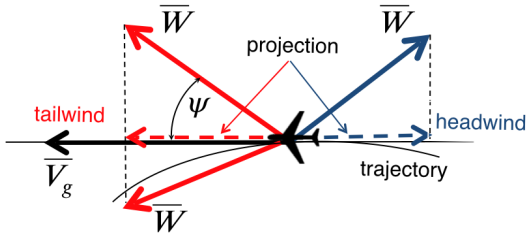

Fig. 9. The concept of wind color-coding.

In turn, the contribution of the solar irradiance is encapsulated by "attaching" a circle to each waypoint with the radius qualitatively proportional to the intensity of the solar contribution; no circles correspond to the night flight.

Figure. 10 illustrates the resulting optimal route (red dots) in comparison with the route along the great circle (blue dots) between the initial and final position of the aircraft for one of the COAMPS wind profiles at 2850 m altitude.

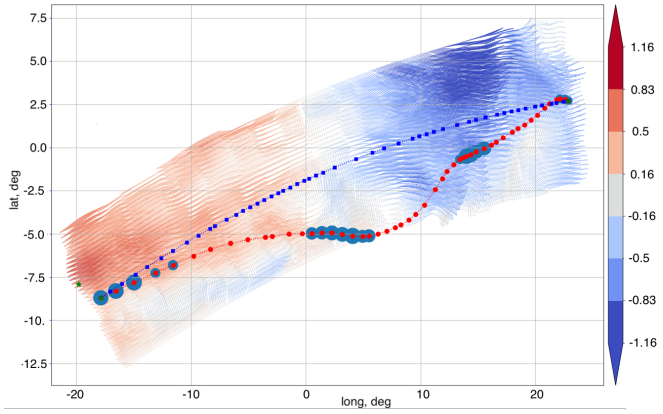

Fig. 10. Comparison of the optimal and great circle routes.

The result illustrates that the optimal route heavily leverages the wind and solar energy sources that provide significant time and energy saving: 1.19 kg of fuel along the optimal route vs 1.45 kg along the great circle, and 73.47 *hours* along optimal route vs 111.48 *hours* along the great circle. The trajectory plot illustrates that the resulting route optimally trades the degree of departure from the shortest flight that increases the flying distance and the intensity of harnessing the tailwind. The route finds, captures, and follows an imaginary stream of wind in the desired direction of flight.

5. CONCLUSION

The key results achieved by the proposed design include the analytical solution of the *minEng* task when all three energy sources are considered simultaneously. The night time dynamics of *minEng* solution is proven to asymptotically approach the non time-varying wind solution (Zermelo's *minT* guidance). The analytical form of the synthesized optimal controls of the bank angle and the commanded airspeed is another key enablers of efficient numerical implementation. Together with the new continuation algorithm, that scales the BVP system with the wind magnitude, the optimal solution became feasible onboard a miniature CPU suitable for aircraft integration.

REFERENCES

Anderson, J.D. (1999). *Aircraft performance and design*. McGraw-Hill, ISBN-13: 978-0070019713.

Beard, R.W. and McLain, T.W. (2012). *Small Unmanned Aircraft: Theory and Practice*. Princeton University Press, ISBN-13: 978-0691149219.

Ben-Asher, J.Z. (2010). *Optimal Control Theory with Aerospace Application*. Education Series. AIAA, https://doi.org/10.2514/4.867347.

Betts, J. (1998). Survey of numerical methods for trajectory optimization. *JGCD*, 21(2), 193–206. doi: 10.2514/2.4231.

Bryson, A. and Ho, Y. (1975). *Applied Optimal Control - Optimization, Estimation, And Control*. Willey, New York, ISBN-13: 978-0891162285.

Burton, M. and Hoburg, W. (2017). Solar and gas powered long-endurance unmanned aircraft sizing via geometric programming. *Journal of Aircraft*, 55(1), 1–10, https://doi.org/10.2514/1.C034405.

COAMPS (1997). The naval research laboratory's coupled ocean/atmosphere mesoscale prediction system (coamps®). Technical report, The Naval Research Laboratory.

Dobrokhodov, V.N., Jones, K.D., Walton, C., and Kaminer, I.I. (2020). *Achievable Endurance of Hybrid UAV Operating in Time-Varying Energy Fields*. AIAA. doi:10.2514/6.2020-2197. URL `https://arc.aiaa.org/doi/ abs/10.2514/6.2020`.

Edwards, D., Kahn, A., Kelly, M., Heinzen, S., Scheiman, D., P.P., Jenkins, Walters, R., and Hoheisel, R. (2016). Maximizing net power in circular turns for solar and autonomous soaring aircraft. *Journal of Aircraft*, 53, 1237–1247. doi:10.2514/1.C033634.

Gardi, A., Sabatini, R., and Ramasamy, S. (2016). Multi-objective optimization of aircraft flight trajectories in the ATM and avionics context. *Progress in Aerospace Sciences*, 83, 1–36.

Hardkernel, L. (2015). User manual odroid-xu4. Technical report, Hardkernel Co, LTD. URL `https://wiki.odroid.com/odroid-xu4/odroid-xu4`.

Hosseini, S. and Mesbahi, M. (2016). Energy-aware aerial surveillance for a long-endurance solar-powered unmanned aerial vehicles. *Journal of Guidance, Control, and Dynamics*, 1980–1993. doi:10.2514/1.G001737.

Kierzenka, J. and Shampine, L.F. (2001). A BVP solver based on residual control and the Maltab PSE. *ACM Trans. Math. Softw.*, 27(3), 299–316. doi: 10.1145/502800.502801.

Klesh, A. and Kabamba, P. (2007). Energy-optimal path planning for solar-poweredaircraft in level flight. *AIAA Guidance, Navigation, and Control Conference and Exhibit*. URL `https://doi.org/10.2514/6.2007-6655`.

Klesh, A. and Kabamba, P. (2009). Solar-powered aircraft: Energy-optimal path planning and perpetual endurance. *Journal of Guidance, Control, and Dynamics*, 32(4), 1320–1329, https://doi.org/10.2514/1.40139.

Longuski, J., Guzmán, J., and Prussing, J. (2014). *Optimal Control with Aerospace Applications*. Number ISBN-13: 978-1461489443 in 32. Springer.

Mathworks (2019). Matlab optimization toolbox. The MathWorks, Natick, MA, USA.

Oettershagen, P., Melzer, A., Mantel, T., Rudin, K., Lotz, R., Siebenmann, D., Leutenegger, S., Alexis, K., and Siegwart, R. (2015). A solar-powered hand-launchable uav for low-altitude multi-day continuous flight. In *Proceedings of IEEE International Conference on Robotics and Automation (ICRA)*, DOI:10.1109/icra.2015.7139756.

Oettershagen, P., Melzer, A., Mantel, T., Rudin, K., Stastry, T., Wawrzacz, B., Hinzmann, T., Alexis, K., and Siegwart, R. (2016). Perpetual flight with a small solar-powered uav: Flight results, performance analysis and model validation. *Proceedings of 2016 IEEE Aerospace Conference*, 10–19, https://doi.org/10.1109/AERO.2016.7500855.

Pontryagin, L.S., Boltyanskii, V., Gamkrelidze, R., and Mishchenko, E. (1962). The mathematical theory of optimal processes, translated by KN Trirogoff. *New York, Wiley*.

Qureshi, B. and Koubâa, A. (2019). On energy efficiency and performance evaluation of single board computer based clusters: A hadoop case study. *Electronics*, 8(2), 182.

Rodionova, O., Sbihi, M., Delahaye, D., and Mongeau, M. (2014). North atlantic aircraft trajectory optimization. *IEEE Transactions o Intelligent Transportation Systems*, 15(5), 2202–2212, https://doi.org/10.1109/TITS.2014.2312315.

SciPy, C. (2019). Scipy reference guide release 0.12.0. URL `http://www.scipy.org/`.

Siegel, C.L. and Moser, J.K. (1995). *Lectures on Celestial Mechanics*, volume 12 of *Classics in Mathematics*. Springer-Verlag Berlin Heidelberg, 1 edition.

Stroman, R., Edwards, D., Jenkins, P., Carter, S., Newton, D., Kelly, M., Heinzen, S., Young, T., Dobrokhodov, V., Langelaan, J., Bird, J., and Reinecke, P. (2018). The hybrid tiger: A long endurance solar/fuel cell/soaring unmanned aerial vehicle. In *48th Power Sources*.

Watson, L. (1990). Globally convergent homotopy algorithms for nonlinear systems of equations. *Nonlinear Dynamics*, 1(2), 143–149, https://doi.org/10.1007/BF01857785.

Wirth, L., Oettershagen, P., Ambühl, J., and Siegwart, R. (2015). Meteorological path planning using dynamic programming for a solar-powered uav. *Proceedings of 2015 IEEE Aerospace Conference*, 10–19, https://doi.org/10.1109/AERO.2015.7119284.

Zermelo, E. (1931). Über das navigationsproblem bei ruhender oder veränderlicher windverteilung. *Z. angew. Math. Mech.*, 11, 114–124, https://doi.org/10.1002/zamm.19310110205.